ELSEVIER

International Journal of Heat and Fluid Flow 21 (2000) 74–83

International Journal of HEAT AND FLUID FLOW

www.elsevier.com/locate/ijhff

Steady and pulsatile flow studies in Abdominal Aortic Aneurysm models using Particle Image Velocimetry

S.C.M. Yu

Thermal and Fluids Engineering Division, School of Mechanical and Production Engineering, Nanyang Technological University, Singapore 639798, Singapore

Received 7 August 1998; accepted 21 July 1999

Abstract

Flow characteristics in Abdominal Aortic Aneruysm models have been investigated using Particle Image Velocimetry over a range of Reynolds numbers (from 400 to 1400) and Womersley numbers (from 17 to 22). Both steady and pulsatile flow experiments have been conducted. For the pulsatile flow, a sinusodial inlet flow waveform $1 + \sin \omega t$ was used. It was found that under the steady flow conditions, a recirculating vortex occupied the entire circular bulge with its core located closer to the distal end of the bulge. The strength of the vortex would increase as the Reynolds number increased but would not exceed more than 10% of the bulk flow in the parent tube. Under the pulsatile flow conditions, the vortex appeared initially near the proximal end of the bulge at the early stage of a flow cycle, occupying approximately 1/4 of the bulge. The subsequent deceleration of the bulk flow caused the vortex to reduce its extent in the direction of the flow but was enlarged in the transverse direction with higher strength. The vortex was convected slowly towards the distal end of the bulge by the bulk flow and an abrupt drop in its strength appeared when it reached there. Attempts have been made to explain the flow development using vortex dynamics.

Notation

A	length of the elliptic bulge in the x direction
D	length of the elliptic bulge in the y direction
d	diameter of the upstream and downstream tube
L	length of the aneurysm
$Q(t)$	volume flowrate (time dependent)
Q_{mean}	mean volume flowrate
Re	$(= U_b D/\nu)$ and the Reynolds number based on the diameter of the tube at 40 mm
T	one period of a cycle
U_b	bulk mean velocity in the upstream tube
x	streamwise direction
y	vertical direction
α	$(= 0.5D(\omega/\nu)^{1/2})$ Womersley number
ν	kinematic viscosity
ω	frequency of each pulsating cycle
ρ	density of the working fluid
θ_o	boundary layer momentum thickness upstream of the aneurysm

1. Introduction

Because pulsatile flow in pipes is an important area of fluid mechanics, several researchers have conducted experimental (Shemer et al., 1985) and computational studies (He and Ku, 1994) in this type of flows. In particular, the growing interest in biofluids engineering in recent years has given impetus to advance research in this area. It is widely considered that pulsatile flow in arteries have to be understood thoroughly before many diseases can be effectively cured, as for example, flows in constriction tubes (stenosis), bifurcating ducts (main systematic arteries from the heart), over cavities (saccular aneurysm) and through sudden expansion (Abdominal Aortic Aneruysm or AAA).

As pointed out by Ku (1997), there are several features of biological flows that can be considered as secondary in importance, such as wall elasticity, non-Newtonian fluid properties (in large arteries: diameter >0.5 mm), slurry particles in the fluid and temperature. As a consequence, many of the investigations can be conducted in the conventional fluid mechanics laboratory (in vitro studies). Non-intrusive measurement techniques, such as the ultrasound anemometer and the laser-Doppler anemometer were commonly used for flow measurements. Particle Image Velocimetry had also been used more frequently in recent years. The advantages of using PIV are numerous. In particular, the ability to capture the entire flow field of interest in any instant of time made it an attractive option to conduct pulsatile flow studies.

E-mail address: mcmyu@ntu.edu.sg (S.C.M. Yu).

0142-727X/00/$ - see front matter
PII: S0142-727X(99)00058-2

When the abdominal aorta walls dilate into a balloon-like bulge, the affected area would be called an Abdominal Aortic Aneurysm (AAA). Many middle aged and old males are at risk for developing AAAs. The abrupt rupture of AAAs usually leads to instant death in up to 90% of the victims. According to statistics, AAAs rupture is the fifteenth leading cause of death in the United States. Bulge diameter is commonly used as a primary indicator of AAA danger. If the AAA diameter exceeds about 5 cm (a health abdominal aorta is about 2 cm in diameter), the AAA must be surgically repaired to avoid abrupt rupture (Johansen, 1982). However, bulge diameter alone may not be the best indication for determination of rupture risk. There are many cases whereby aneurysms rupture at diameters less than 5 cm, for example see Darling (1970).

It is, therefore, clear that there is a need for more understanding of the flows in artery with AAA. Majority of the previous research works on AAA were conducted using flow visualization methods, for example, Fukushima et al. (1989). LDA and color Doppler flow imaging techniques were also used to study the steady flow characteristics, see for example, Budwig et al. (1993), Peattie et al. (1994) and Asbury et al. (1995). More recently Bluestein et al. (1996) employed Digital Particle Image Velocimetry to study the flow inside the aneurysm under the steady flow conditions. Table 1 provides a summary of some recent experimental studies on AAAs. It should be pointed out that it is also relatively common to use steady flow results to extrapolate the analysis for pulsatile flows. However, as it will be shown later, the pulsatile flow results only resembled those of steady ones less than 1/5 of a cycle. The steady flow results tend to underestimate the effects of flow recirculation.

As shown in Table 1, the present experiments differ from those of the previous ones in three aspects. First, both steady and pulsatile flow experiments have been conducted simultaneously. Second, physiological wave forms have not been used in the present experiments although they could be improvised easily by modifying the cam shape (see the subsequent section for details). It was felt that a relatively simple wave form should be sufficient for any preliminary comparison with CFD results. Finally, the Reynolds number range investigated was well below the critical value at which transition to turbulent flow occurred. The effects of turbulence transition will be dealt with in a future communication. To minimize light distortion at the air/solid/liquid interfaces, a mixture of glycerin and water has been used as the working fluid.

The following section describes briefly the experimental set-up including the Particle Image Velocimetry system for obtaining velocity measurements. It will be followed by presentation and discussion of the results. The paper ends with a summary of important findings.

Table 1
Summary of recent experimental investigation on AAA flow

	Fukushima et al. (1989)	Budwig et al. (1993)	Peattie et al. (1994)	Asbury et al. (1995)	Bluestein et al. (1996)	Egelhoff et al. (1997)	Present analysis
Flow condition	Pulsatile (physiological wave forms)	Steady	Steady	Steady	Steady	Pulsatile (physiological wave forms)	Steady/Pulsatile (sinewave forms)
Instrumentation	Flow visualization	LDA	Color Doppler flow imaging	Color Doppler flow imaging	DPIV	Flow visualization	PIV
Reynolds (Re) and Wormersly (α) numbers	$289 < Re < 3410$ $4.07 < \alpha < 10.6$	$400 < Re < 1800$	$1050 < Re < 4350$	$500 < Re < 2600$	$300 < Re < 3600$	$362 < Re < 5695$ $16.4 < \alpha < 21.2$	$726 < Re < 1274$ $17 < \alpha < 22$
Critical Reynolds number	NA	$2000 < Re < 2500$	$1600 < Re < 2750$	$2000 < Re < 2500$	NA	$2000 < Re$	NA

2. Flow configurations and instrumentation

2.1. Test rig

A test rig has been set up, as shown in Fig. 1(a). The flow was delivered by a submersible pump to the test section through a head tank, a flow straightener and a settling chamber in which five fine screens were housed. A uniform inlet flow with thin boundary layers was ensured by a bell-shape contraction cone of 5:1 area ratio. The instantaneous flowrate passing through the test section was measured by a electro-magnetic flowmeter (EFM) (Rosemount, Model 8722) and monitored by a digital oscilloscope (Tektronic model 3840) located downstream of the test section.

A small piston-cylinder pump driven by a DC gear-motor (Bordine) fitted with a circular cam was used to generate the

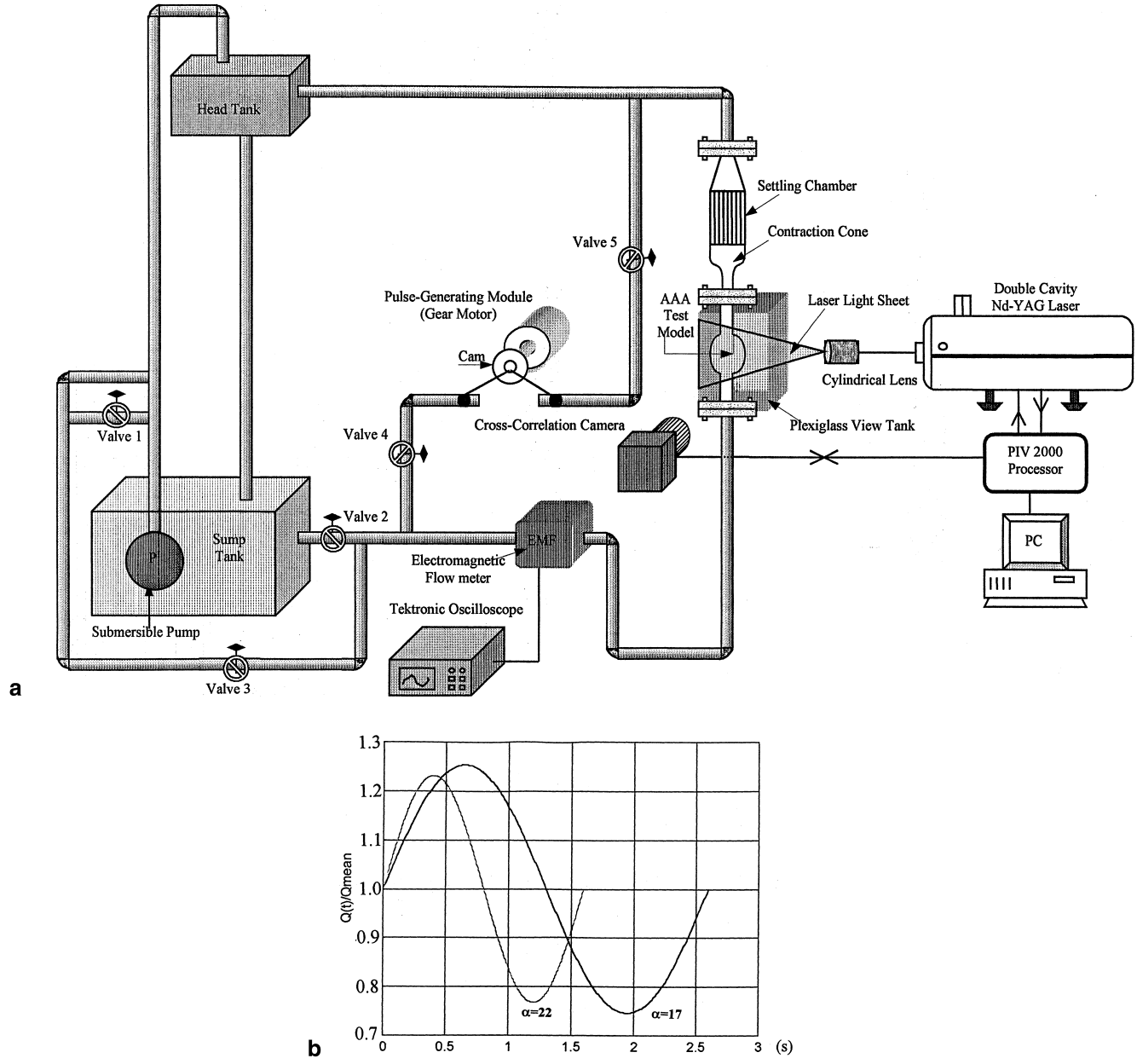

Fig. 1. (a) Schematic of the test rig; (b) inlet flowrate waveforms for Run I ($\alpha = 17$) and Run II ($\alpha = 22$).

necessary pulsating flow conditions. Typical volume flowrate patterns are shown in Fig. 1(b) in which the tested mean, peak and minimal Reynolds numbers in the tube were at 1000, 726 and 1162 respectively (for the smaller amplitude wave). It should be noted that the same test rig was used to study steady flows by closing the valves located before and after cylindrical pump. In the present investigation, a solution mixture of glycerin and water (viscosity and density at 3.5 cp and 1.121 g/cm^3, respectively) was used as the working fluid. Table 2 summarizes the testing conditions which are to be presented in the present communication.

2.2. Test sections

Altogether three models made of pyrex glass tubes (2 mm thick) had been used. Model 1 was a straight tube of 40 mm internal diameter and a length of 300 mm. As shown in Fig. 2, two geometries of the AAA were studied. Both of these geometries may be described as a straight tube with a concentric bulge. The geometry of the bulge can be described by the formula representing an ellipse, i.e.

Table 2
Flow conditions under investigation

Steady flow	
Re	400–1400
Pulsatile flow	(run I)/(run II)
Re (maximum)	1162/1274
Re (average)	1000
Re (minimum)	726/838
Womersley number	17/22

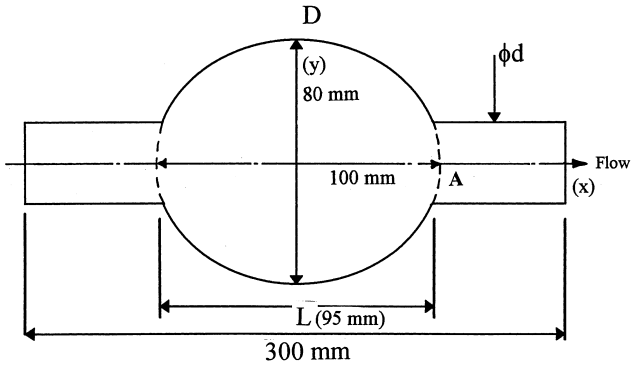

Fig. 2. Schematic diagram of models tested (cf. Table 3).

$$\left(\frac{x^2}{(A/2)^2}\right)+\left(\frac{y^2}{(D/2)^2}\right)=1,$$

where A and D are 100 and 80 mm respectively for the developed AAA. The dimensions are further summarized in Table 3.

For pulsatile flow, the two dimensionless parameters commonly used to characterize the flow conditions are the Reynolds number ($Re=U_bD/v$) and the Womersley number (Womersley, 1955) ($\alpha=0.5D(\omega/v)^{1/2}$ where ω is the frequency of the cyclic variation). While the Reynolds number is a comparison of inertial force to viscous force, the Womersley number can be interpreted as the ratio of the unsteady force to viscous force. In general, high Womersley number (>10) flows correspond to situations involving periods of rapid acceleration and deceleration.

A plexiglass box of dimensions 180 mm × 100 mm × 100 mm was constructed to house the region of interest in each of the two models. The same liquid mixture as the working fluid was filled into the box so that optical distortion and reflection could be greatly minimized at the glass/liquid interfaces.

2.3. Particle Image Velocimetry

Particle Image Velocimetry (PIV) system (Dantec FlowMap PIV system, Dantec Measurement Technology, Denmark) was used to obtain the velocity information in conjunction with a coherent frequency doubled ($\lambda=532$ nm) Nd : YAG laser (cf. Fig. 1(a)). The Nd : YAG laser is capable of producing 200 mJ at 532 nm and has a pulse rate of 10 Hz with a 9 ns duration, effectively freezing the flow. The output of the light beam was diffracted by a cylinderical lens such that a thin (maximum 1 mm) laser light sheet could be placed in the vertical ($X-Y$) plane of the model. Up to 2000 vectors per second can be processed on-line by the accompanied hardware (PIV 2000 Processor) and software (FlowManager). A Nikon AF Micro-Nikkor lens (60/2.8) had been used for focusing in the experiments. The displacements of the particles are obtained by locally cross-correlating sequential images recorded by a CCD camera (80C42 DoubleImage 700). The velocity vector fields are then computed from the known time interval between two pulses of the Nd : YAG laser. The cross-correlation function of the two samples was calculated using FFT techniques. The activation of the laser pulse was externally triggered by the signals from the oscilloscope which sychronized with the variation of the flowrate measured by the Electromagnetic Flowmeter. Nylon Powder (SG = 1.1, Dantec Measurement Technology, Denmark) of 50 μm diameter was used to seed the flow. Further details of the system can be found in Yu (1998).

Table 3
AAA model geometry

Model (#)	L/d	D/d	D/A	Axisymmetric
Straight tube (1)	0	1.0	0.4	Yes
Distended AAA (2)	2.2	1.7	0.68	Yes
Developed AAA (3)	2.2	2.0	0.8	Yes

3. Results and discussions

Only the most representative results are shown here. Some of observations and comments made in the following text were actually deduced from results obtained from a wider range of flow conditions.

3.1. Steady flow

For the baseline model at $Re=1000$ and Fig. 3(a), a large potential core existed across the tube with very thin boundary layers formed at the walls (thickness was at about 5% of the

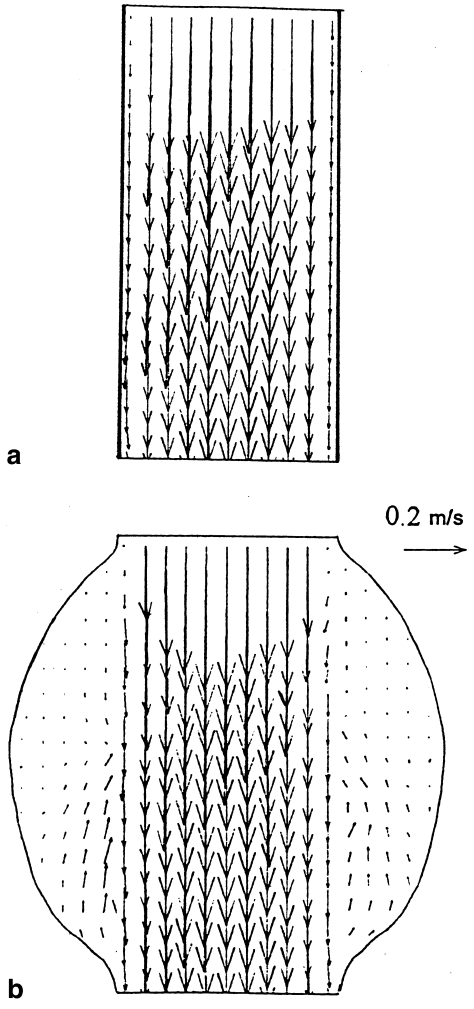

Fig. 3. Velocity vector plots at the symmetry plane for (a) Model 1 and (b) Model 3, under steady flow condition, $Re=1000$.

diameter). The same trend prevailed within the range of Reynolds numbers investigated.

For the AAA model (Model 3) in Fig. 3(b), the upstream flow conditions before entering the bulge consisted of a large potential core across the duct indicating that an extremely thin boundary layer at the wall existed. The general flow feature within the bulge mainly consisted of a jet of fluid flanked by weak recirculation vortices on both sides. The flow recirculation was a consequence of the adverse pressure gradient imposed by the increase in cross-sectional area at the bulge. The core flow was steady and did not spread noticeably outward as it moved toward the end of the bulge. The strength of the velocity inside the recirculation had a maximum of 0.08 U_{bm}. It is also noticed that the vortex core was located closer to the downstream side of the bulge. Reducing the size of the bulge (i.e., Model 2) did not change the flow features dramatically. The results obtained here are similar to those obtained by Budwig et al. (1993) even with a different initial condition (for the case of Budwig et al. (1993), a fully developed inlet condition was used).

3.2. Pulsatile flow

In the following discussion, the beginning of the wave is at the average flowrate point and is followed by the acceleration towards the first peak. The duration of each cycle was about 2.5 and 1.5 s for Run I and II, respectively. Figs. 4 and 5 show the vector plots for the baseline tube (Model 1) and Model 3 at Run II (cf. Table 2).

For the baseline tube in Fig. 4, as may have been expected, the acceleration of the flow was accompanied by a corresponding decrease in boundary layer thickness (less than 5% of the diameter in Fig. 4(a)). After the peak phase, the flow began to decelerate, with a consequence of thickening of the boundary layers (to about 8% of the diameter in Fig. 4(b)). When reaching the minimal flow condition, the flow remained attached to the wall (Fig. 4(c)).

For Model 3 in Fig. 5, a very weak recirculation vortex was formed, at the very early stage in each cycle, close to the proximal end of the bulge (Fig. 5(a)). Maximum velocity was at about 5% of the bulk mean velocity in the parent tube, i.e. at the same order of magnitude to that found in the steady flow case. The flow pattern did not change tremendously except that the recirculating vortex appeared to grow slightly stronger as the flow continued to accelerate towards the peak flowrate point (Fig. 5(b) and (c)). After passing through the peak flowrate point and as the flow began to decelerate, the strength of the recirculating vortex increased and the vortex core was seen moving towards the center plane of the bulge (Fig. 5(d) and (e)). As it will be shown later, it is the result of the deceleration effects due to the increase in bulge diameter as well as the cyclic variation (deceleration) of the flow causing the vortex strength to increase. After passing through the average flowrate point, the vortex core was found to migrate further downstream towards the distal end of the bulge (Fig. 5(f)). The strength of the vortex appeared to reach its maximum at about $t/T = 0.7$ (Fig. 5(g) and (h)). At this phase, the vortex was actually very close to the distal end of the bulge. It should be noted that the traverse extent of the vortex grew as the strength of the vortex increased. As such, there was a higher velocity region in the passage between the vortices. After passing through the minimum flowrate point, as the flow began to accelerate, the vortex tended to decay rapidly and at the same time its core moved closer to the distal end (Fig. 5(i)). The continuous flow acceleration, as the waveform traveled towards the average flowrate point, the strength of the vortex near the distal end drop abruptly and a weak circulating vortex began to form at the proximal end (Fig. 5(j)). The above

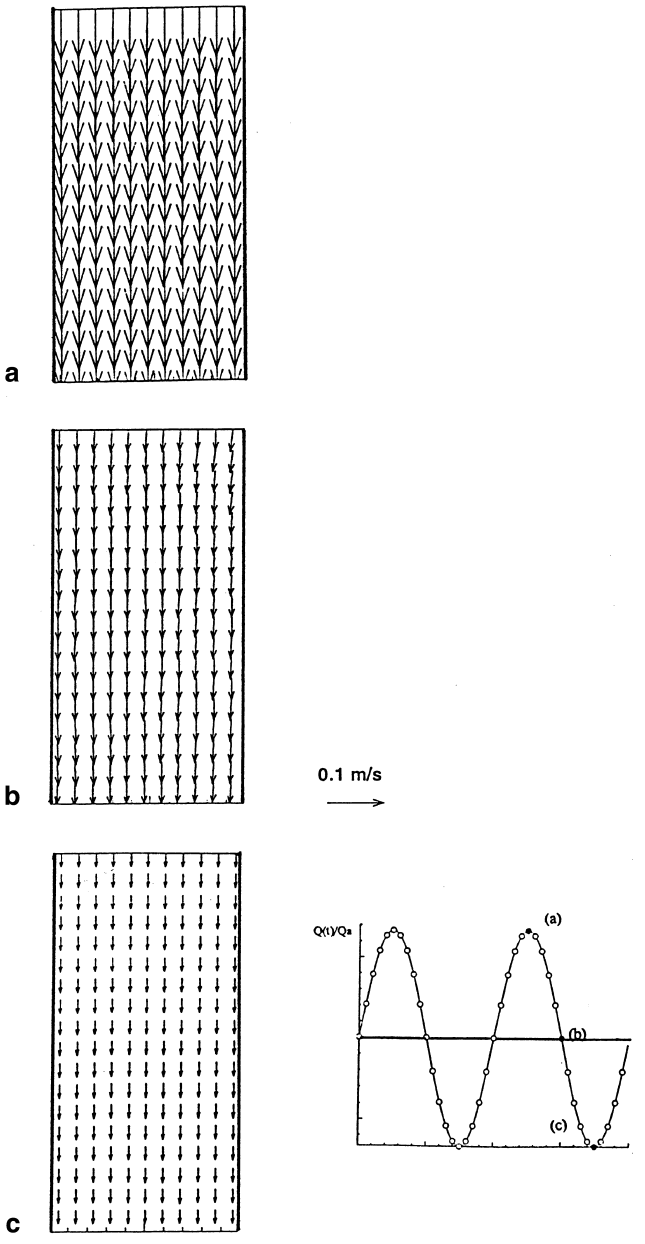

Fig. 4. Velocity vector plots at the symmetry plane for Model 1 under pulsatile flow condition at $\alpha = 22$.

sequence (Fig. 5(a)–(j)) repeated itself in the subsequent cycle. It is interesting to note that inside the aneurysm and at the minimal flow condition, the strength of the vortex was much higher than that at the peak flow condition (compare Fig. 5(c) and (i)) in particular near the distal neck.

3.3. Effects of aneurysm sizes

In general, the two models tested do not show significant difference from each other for all the flow conditions considered. However, it appears that the strength of the vortex was weaker if the size of the bulge was smaller, by about 20% at every point over a cycle. The decay rate for the vortex however was also less rapid for the smaller bulge. As shown in the numerical investigation on AAA steady flow by Budwig et al. (1993), when D/d is larger than 1.3, the flow characteristics

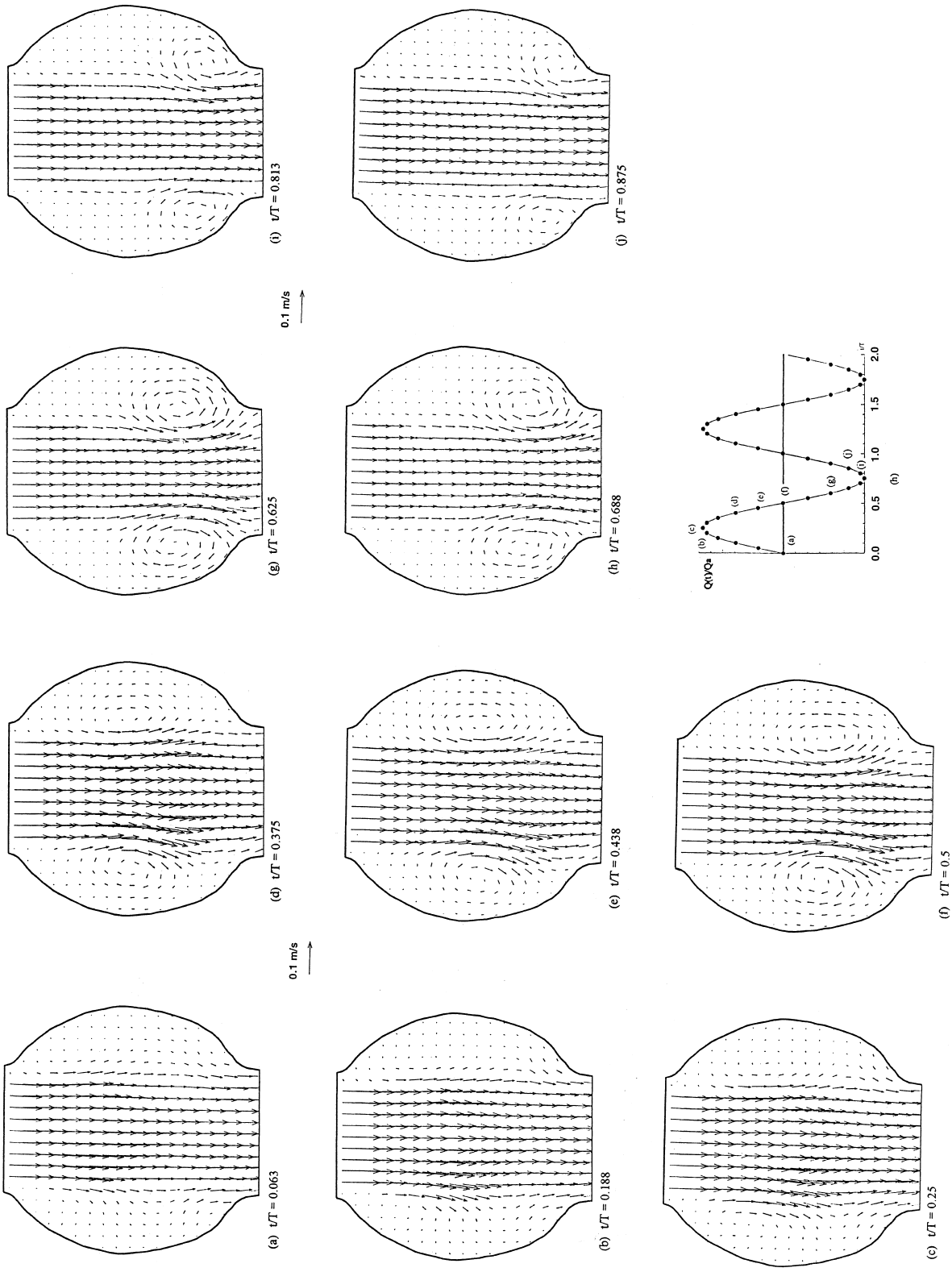

Fig. 5. Velocity vector plots at the symmetry plane for Model 3 under pulsatile flow condition at $\alpha = 22$.

would become qualitatively similar. It may be early to reach the same conclusion based only on the two models tested for pulsatile flows here. More works are required to validate this.

3.4. Effects of Womersley number

The flow patterns found in Run I were quite different from those of Run II. As shown in the waveform of Run I and II in Fig. 1(b), the slopes for the flow acceleration and deceleration are actually steeper at higher Womersley number. As such, a very weak vortex was formed near the proximal neck at the early stage of the cycle for Run I, see Fig. 6(a). The vortex maintained nearly the same strength and size to around the maximum flowrate point (Fig. 6(b)). After passing through the maximum flowrate point and as the flow decelerated, the vortex started to migrate towards the distal end of the bulge. The vortex reached its maximum strength when the flowrate was reduced to the average flowrate point (Fig. 6(c)). The vortex strength decreased further when the flowrate was reduced to a little bit higher than minimum flowrate point (Fig. 6(d)). It should be noticed that the transverse extent of the vortex did not enlarge into the parent tube as in the case of Run II. At the beginning of the acceleration phase and as the flowrate increased, similar to those found in the case of Run II, the vortex was quickly dissipated at the distal end of the bulge. Before the flowrate reached the average flowrate point again, the vortex almost dissappeared (Fig. 6(e)) and the above sequence repeated itself thereafter.

It appears that the major difference between the two cases is mainly on the flow development during the deceleration phase. For the lower Womersley number case (Run I), the flow did not decelerate (or the adverse pressure gradients created by the deceleration of the flow) fast enough to enable the formation of a vortex as strong as the higher Womersley number case.

3.5. Differences between steady and pulsatile flow

Important differences were observed between steady and pulsatile flows from the preceding sections. Under pulsatile flow conditions, the location of the center of the vortex was not constant (i.e., very close to the proximal neck) within the range of Reynolds numbers investigated. For the steady flow case, the location of the vortex is rather steady. Thus, the regions of high shear stresses and low shear stresses were not permanent, and wall shear stress oscillation could appear. In particular, the highest magnitude of shear stresses in general appeared closer to the distal end of the bulge during a certain period of a cycle (from about $t/T = 0.3$ to 0.8). During this period, the flow feature was only qualitatively similar between the steady flow and pulsatile flow regimes. However, the magnitude of the shear stress would be very much underestimated by the steady flow results. This observation clearly suggested that it is not appropriate to use the steady flow results to extrapolate to the analysis for the pulsatile counterpart.

3.6. Further discussion

The term separation is commonly used to denote the initial appearance of eddy of recirculation flow on the wall. However, as it has been mentioned earlier, the near wall resolution for the present experiment was not desirable and it is difficult to define the exact location of the separation point. It may therefore be convenient to discuss in general terms the sequence of observed events for a pulsatile cycle in terms of vortex dynamics. As shown schematically in Fig. 7(a), at the beginning of the cycle, a weak vortex [1] was formed very close to the proximal end of the bulge. A situation reminiscent of flow over a backward facing step. The streamwise extent of the vortex occupies about one quarter of the bulge. Although the bulk flow is actually accelerating, the increase in bulge diameter provides an adverse pressure gradient which in turn decelerates the flow. It should be noted that the adverse pressure gradient created during the deceleration phase of the flow cycle is also important to the flow development. It is the balance of the two effects (acceleration and deceleration) which determine the flow development through the AAA. It appears that the latter has a relatively stronger effect on the flow causing it to separate and roll into a vortex at the beginning of a cycle. During the acceleration phase of the cycle, the flow pattern does not change dramatically and the location of the vortex is very steady. The vortex strength begins to increase as the flow starts to decelerate (Fig. 7(b)). The vortex core is shifted downstream towards the center plane of the bulge and by about $t/T = 0.5$, the vortex core is at the center plane. This is an obvious effect of the adverse pressure gradient becomes more dominant as the flow decelerates (i.e. when the effects of acceleration disappeared). It should be noted that though the flow decelerates, the bulk flow is still going forward. As shown in Fig. 5 that the variation of vortex strength within a cycle, the strength actually increased sharply during the deceleration phase and continued to increase until almost the end of the cycle where an abrupt drop in strength was found. By examining the vector plots in Fig. 5 closely, it was found that from $t/T = 0.5$ onward, two important effects were observed. First, the vortex was first intensified and was then convected further downstream towards the distal end. Second, there was a rapid drop in the strength of the vortex as it reached the distal end.

For the convection of the vortex downstream, a simple explanation can be given in terms of the induced velocities of the streamwise vortex pairs. Consider the vortex pair with equal and opposite strength $\pm\Gamma$ and spaced $2a$ apart, as sketched in Fig. 7(c). Recall from the vortex dynamics that both the vortices will move to the right with a speed equal to $\Gamma/4\pi a$ (Eskinaki, 1967). The fluid between them will also be ejected to the right at about four times this speed. Therefore, the dynamics of the pair of vortices would tend to (i) move forward towards the distal end and (ii) cause the fluid between them to be ejected at higher speed. Subsequent examination on the vector plots at around $t/T =$ 0.5–0.6 (for example, see Fig. 5(g)) confirmed our speculation that the flow between the two vortices were actually higher than anywhere within the flowfield.

As to the intensification of the pair of vortices, postulation can only be given as below. Consider the vortex pair as part of a vortex ring for the entire 3-D bulge, as sketch in Fig. 7. As the vortex pair is moving slowly towards the center plane of the bulge where the cross-sectional area is relatively larger. In order to perserve the angular momentum, the vortex ring would be "stretched" causing the circulation strength to increase (i.e. Fig. 7(a) to (b)). After passing through the center plane, a reversed situation occurred. As the vortex ring moves towards the distal end, the vortex tube will be compressed due to the contraction effects (i.e. Fig. 7(b) to (c)). As a consequence, the strength of the circulation decays rapidly as the vortex ring arrived at the distal end. It must be pointed out that the intensification of the vortex ring does not occur exactly at the center plane of the bulge but is at a small distance

[1] It can be seen as a vortex ring if the entire 3-D AAA model is considered.

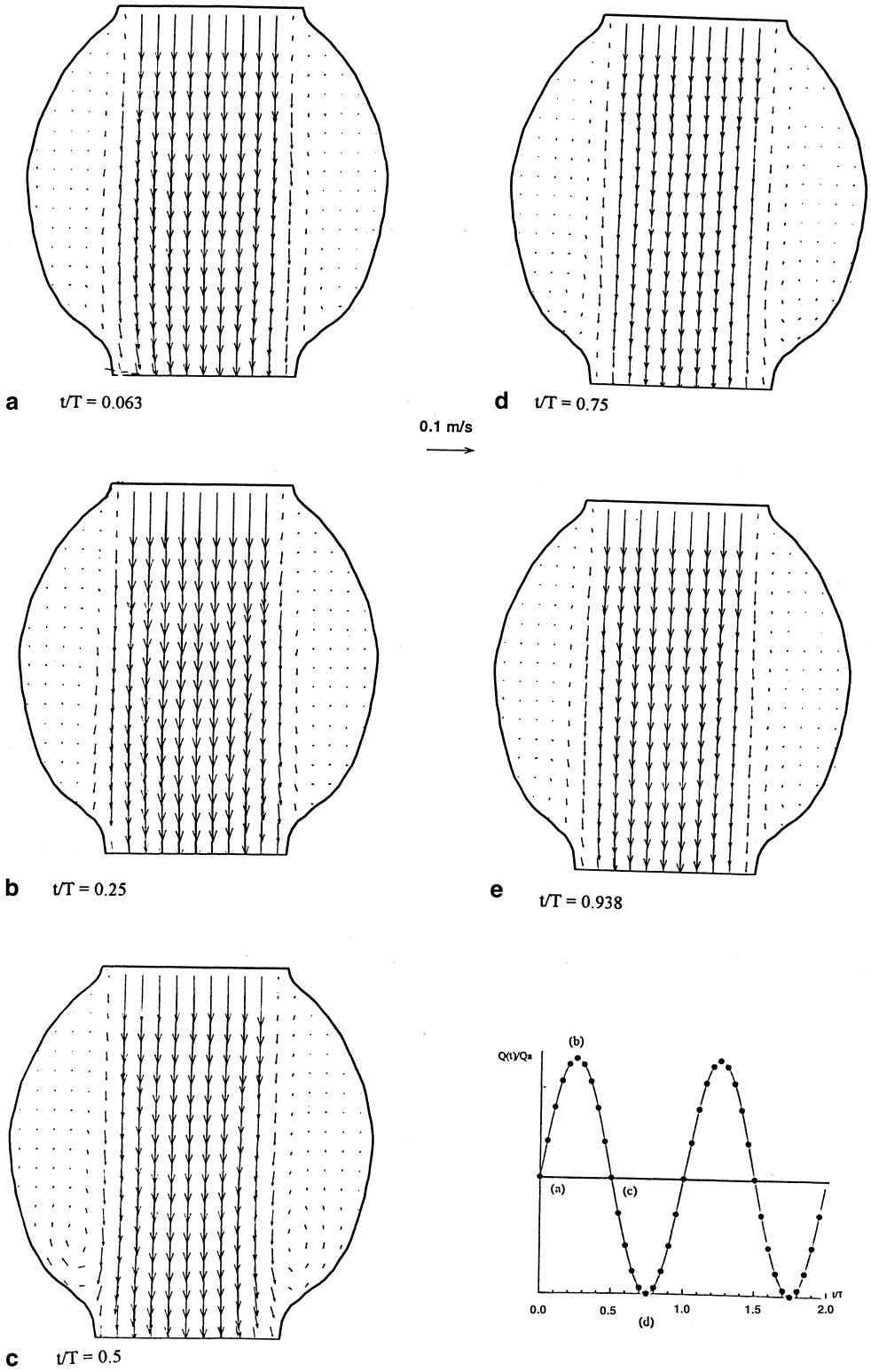

Fig. 6. Velocity vector plots at the symmetry plane for Model 3 under pulsatile flow condition at $\alpha = 17$.

inside the contracting part of the bulge. Apparently, there is a time lag between the two events.

It should be noted that the above analysis on the flow had so far disregarded the effects of viscosity. The viscous effect can be important both during the stretching of the vortex in the first half of the bulge and its subsequent compression in the second half of the bulge. For the former, the viscous effect generally facilitates the boundary layer growth and thereby the strength of the vortex ring when it is being stretched subsequently. This may explain in part why the intensification of the vortex ring overshot into the contracting part of the bulge. However, as the vortex ring is being compressed in the second

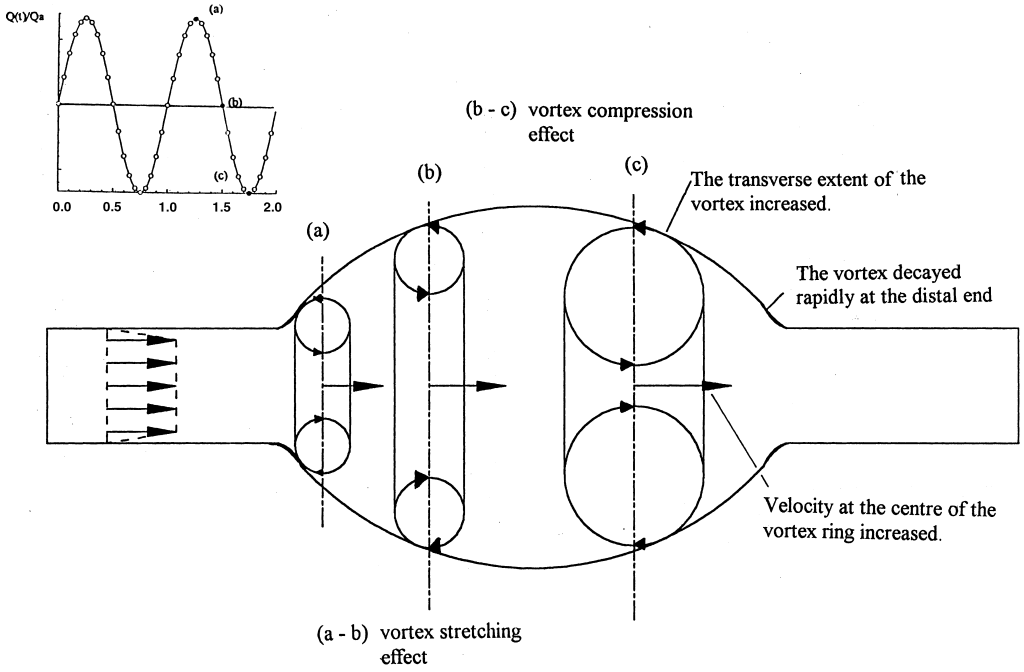

Fig. 7. Schematic of the vortical structure inside the AAA at $\alpha = 22$.

half of the bulge, the viscous effect would tend to enhance the decay of the vortex strength further. This may lead to the eventual disappearance of the vortices at the distal end of the bulge.

The size of the bulge does have an important effect to the formation and the subsequent development of the vortex ring. As shown by the results in Model 2, although the flow patterns are very similar to that of Model 1, the strength of the circulation is higher by about 20%. It is also interesting to note that by reducing the Womersley number, the same effects can also be observed even in Model 1. It appeared that the formation of the vortex ring is closely associated with the rapid acceleration and deceleration of the bulk flow. However, more future works are needed to examine the full impact of the Womersley number effects.

4. Concluding remarks

Particle Image Velocimetry has been used to study the pulsatile flow characteristics in two Abdominal Aortic Aneruysm or AAA models with an input sinewave form and over a range of Reynolds and Womersley numbers. The present investigation attempted to provide a better understanding of the flows with AAA. It was found that under the steady flow conditions, flow recirculation occupied the entire bulge with the vortex core located closer to the distal end. The strength of the velocity inside the recirculation zone is less than 10% of the bulk mean flow. For the pulsatile flow, recirculation appeared initially at the upstream side of the bulge at the early stage of each flow cycle, occupying approximately 1/4 of the bulge. As the bulk flow continues to decelerate, the extent of the recirculation increased and the core of the vortex was shifted towards the center plane of the bulge. Two important effects on the recirculation region were observed as the bulk flow decelerated. First, the strength of the recirculation was strengthened. Second, the flow recirculation reduced its extent in the direction of the flow but was enlarged in the transverse direction. Based on the analysis using inviscid vortex dynamics, the vortex was strengthened due the vortex stretching effects as the vortex ring goes from the proximal end to towards the center plane. After passing through the center plane and as the vortex ring moved towards the downstream side of the bulge, an abrupt drop in its strength appeared due to the vortex compression effects. The strength of the vortex was found to dissipate quickly after the vortex ring arrived at the distal end.

Acknowledgements

The author would like to acknowledge the financial support to this project from the Academic Research Grant Committee.

References

Asbury, C.L., Rwberti, J.W., Bluth, E.I., Peattie, R.A., 1995. Experimental Investigation of Steady flow in rigid models of Abdominal Arotic Aneurysms. Annals of Biomedical Engineering 23, 29–39.

Bluestein, D., Niu, L., Schoephoerster, R.T., Dewanjee, M.K., 1996. Steady flow in an aneurysm model: correlation between fluid dynamics and blood platelet deposition. ASME Journal of Biomechanical Engineering 118, 280–286.

Budwig, R., Elger, D., Hooper, H., Slippy, J., 1993. Steady flow in abdominal aortic aneurysm models. ASME Journal of Biomechanical Engineering 115, 418–423.

Egelhoff, C.J., Budwig, R.S., Elger, D.F., Khraishi, T.A., 1997. A model study of pulsatile flow regimes in abdominal aortic aneurysms. ASME FEDSM97-34-31, ASME Fluids Engineering Division Summer Division Meeting.

Darling, R.C., 1970. Ruptured arteriosclerotic abdominal aortic aneurysms: a pathologic and clinical study. American Journal of Surgery 119, 397–401.

Eskinaki, S., 1967. Vector Mechanics of Fluids and Magnetofluids. Academic Press, New York.

Fukushima, T., Matsuzawa, T., Homma, T., 1989. Visualization and finite element analysis of pulsatile flow in models of the abdominal aortic aneurysm. Biorheology 24, 109–130.

He, X., Ku, D.N., 1994. Unsteady entrance flow development in a straight tube. ASME Journal of Biomechanical Engineering 116, 355–360.

Johansen, K.H., 1982. Aneurysms. Scientific American 247, 110–125.

Ku, D.N., 1997. Blood flow in arteries. Annual Review of Fluid Mechanics 29, 399–434.

Peattie, R.A., Schrader, T., Bluth, E.I., Comstock, C.E., 1994. Development of turbulence in steady flow through models of abdominal aortic aneurysms. Journal of Ultrasound Medicine 13, 467–472.

Shemer, L., Wygnanski, I., Kit, E., 1985. Pulsatile flow in a pipe. Journal of Fluid Mechanics 153, 313–338.

Womersley, J.R., 1955. Method for calculation of velocity, rate of flow and viscous drag in the arteries when the pressure gradient is known. Journal of Physiology 127, 553–563.

Yu, S.C.M., 1998. Experimental investigation of pulsating and rotating flows. Applied Research Project Final Report (RG 29/96), School of Mechanical and Production Engineering, Nanyang Technological University (available on request).